Polymer Chemistry

ROYAL SOCIETY OF CHEMISTRY

PAPER

View Article Online
View Journal | View Issue

Cite this: *Polym. Chem.*, 2024, **15**, 2981

Crosslinked siloxane–silsesquioxane elastomer with pyrene functionalization for rapid adsorption of benzene, toluene, and xylene (BTX) from water and sensing of charged species†

Teeraya Bureerug, [a] Chidchanok Wannasiri,[a] Supphachok Chanmungkalakul, [a] Mongkol Sukwattanasinitt,[b] Vuthichai Ervithayasuporn *[a] and Thanthapatra Bunchuay *[a]

A crosslinked siloxane/silsesquioxane elastomer with pyrene functionalization (**Py-CSSE**) was rapidly synthesised within 10 minutes *via* a one-pot multicomponent anionic ring-opening polymerization between octamethylcyclotetrasiloxane (**methyl D_4**), octavinylsilsesquioxane (**OVS**) and a mono-pyrene functionalized SQ cage (**Mono-PySQ**). The structural characterization of **Py-CSSE** was conducted using MAS solid-state ^{29}Si and ^{13}C NMR, FTIR, and PXRD techniques. Furthermore, an examination of the mechanical and thermal characteristics was conducted using TGA, DSC, and compressive tests. **Py-CSSE** demonstrated significant elasticity (a strain of 60% and a pressure of 0.5 MPa) and quickly returned to its former shape without any cracking, even when subjected to a pressure range of up to 40% strain for 3 cycles. The pyrenyl moieties permitted a strong blue fluorescence emission in both the solid-state and in suspension in an organic solvent. The presence of silsesquioxanes, siloxanes, and pyrene moieties concomitantly facilitated its use in cation (Cu^{2+}) and anion (F^- and CN^-) sensing in polar organic solvents. Importantly, **Py-CSSE** exhibited efficient adsorption of benzene, toluene, and xylene (**BTX**) by showing a remarkably high adsorption capacity in the range 28–34 mmol g^{-1}. **Py-CSSE** exhibited ultrafast adsorption of **BTX** by showing complete removal of *o*-xylene within 90 seconds. Furthermore, **Py-CSSE** surpassed other porous materials in terms of **BTX** adsorption performance and showed exceptional recyclability for **BTX** removal, maintaining adsorption effectiveness for at least 5 cycles.

Received 10th April 2024,
Accepted 8th June 2024

DOI: 10.1039/d4py00394b

rsc.li/polymers

Introduction

Over the past few decades, rapid urbanization and industrialization have contributed to serious environmental problems such as water pollution. Aromatic hydrocarbons, particularly benzene, toluene, and xylene (**BTX**), are a major class of chemical contaminants as a result of their toxicity and carcinogenicity.[1,2] Exposure to these compounds in even small amounts can cause adverse effects on both land-based and aquatic ecosystems. **BTX** water pollution is mostly caused by petroleum leakages from underground storage tanks, urban garbage, and the chemical industry. Various conventional methods can be used to remove **BTX** from water and wastewater, including adsorption, aeration, biological oxidation, and chemical oxidation.[3,4] Undeniably, chemical adsorption utilising porous materials is a powerful and widely employed technique in practical applications.[5–8]

Silica, or SiO_2, makes up a significant proportion of the Earth's crust, accounting for approximately 60% of its composition. Because it is inexpensive and readily available, silica is commonly used as a chemical adsorbent and as a stationary phase in column chromatography.[9,10] However, the strong Si–O covalent bonds make it insoluble in both common organic solvents as well as water, providing difficulties for mechanistic investigations of chemical reactions occurring on the silica surfaces and at the silicon center.[11,12] As an alternative, attention has turned to employing silsesquioxanes (**SQs**), hybrid organic–inorganic silicon materials, as representative models for silica. The core structure of **SQs** comprises inorganic Si–O–Si units that are chemically functionalized with diverse organic residues (R groups), enabling subsequent modifications

[a]*Department of Chemistry, Center of Excellence for Innovation in Chemistry (PERCH-CIC), Faculty of Science, Mahidol University, Rama VI Road, Ratchathewi, Bangkok 10400, Thailand. E-mail: thanthapatra.bun@mahidol.edu, thanthapatra.bun@mahidol.ac.th*
[b]*Department of Chemistry, Faculty of Science, Chulalongkorn University, Bangkok, 10330, Thailand*

† Electronic supplementary information (ESI) available. See DOI: https://doi.org/10.1039/d4py00394b

through various organic reactions.[13–16] Furthermore, **SQ**-based materials with highly symmetrical cage-type structures, such as polyhedral oligomeric silsesquioxanes (**POSS**s), have shown enhanced physico-chemical characteristics compared to other silicon-based materials and have become promising contenders for various applications, for example, **POSS**s have been utilized as fillers in composite materials as a result of their nano-sized cage structures, thermally robust and elastic behavior,[17–19] flame retardancy,[20,21] and mechanical strength.[22,23] These features have highlighted **POSS**s as potential high-performance electrode materials for supercapacitors[24] and lithium-ion batteries.[25–27] In addition, **POSS**s can be utilized to augment the hydrophobic properties and regulate the swelling capacity of hydrogels in the field of biomedical and coating applications.[28–32]

Recently, our group reported an ultrafast synthesis of a superhydrophobic **SQ**-based elastomer from the base catalysed condensation reaction of a cyclic siloxane (**methyl D_4**) with octavinylsilsesquioxane (**OVS**).[33] The reaction reached completion in a time span of only 15 minutes, resulting in the formation of homogeneous micro-ring elastomers that had exceptional mechanical properties and exhibited oil and non-polar solvent adsorption. The hydrophobicity of the elastomer presumably derived from the alkyl moieties appended on the silicon centers of both **methyl D_4** and **OVS**. In addition, functionalization of the **POSS** with the electron-withdrawing pyrenyl and anthracenyl fluorophores resulted in the creation of electron deficient silicon centers that showed strong affinity for the recognition and detection of fluoride, cyanide, and hydrogen phosphate in polar organic solvents.[34–37] Importantly, the excimer emission mode of these fluorophores can be modulated in the presence of guest molecules, enabling their utility in detection of diverse chemical species including gases, organic compounds, and ions. Moreover, its high electron mobility and efficient light emission make it a promising candidate for fluorescent sensors.[38] Taking inspiration from these previous results, our group aims to apply this established synthetic methodology to incorporate fractions of organic fluorophores into the elastomer in order to prepare fluorescent silicon-based hydrophobic elastomers capable of adsorption and sensing applications. A typical procedure utilized for retaining high elasticity and tunable photophysical and mechanical properties is the covalent cross-linking of fluorophores to elastomers.[39] For instance, Craig and co-workers synthesised stress-responsive polysiloxanes by treating mechanoacid diene and rhodamine dye derivatives with poly(dimethylsiloxane) (PDMS).[40] Brook and co-workers synthesised luminous silicon elastomers by coupling **NH_2-PDMS-NH_2** with an aldehyde-modified tetraphenylene derivative *via* the imine condensation reaction.[41]

Herein, we present a one-pot synthetic methodology for preparing a fluorescent pyrene functionalized silicon-based hydrophobic elastomer (**Py-CSSE**) *via* the base catalysed anionic ring-opening polymerization reaction of three chemical components including **methyl D_4**, **OVS**, and the mono-pyrene substituted **OVS** (**Mono-PySQ**).[42] Under the specific reaction conditions, the crosslinked fluorescent elastomeric products were obtained within 10 minutes with the outstanding yield of 83%. The presence of pyrenyl substituents significantly modulated the chemical properties of the resulting materials for chemical adsorption applications and also turned-on fluorescent properties for sensing. **Py-CSSE** exhibited outstanding performance in **BTX** adsorption by showing adsorption capacities for benzene, toluene, *o*-xylene, *m*-xylene, and *p*-xylene of 2.65, 2.98, 3.23, 3.07, and 3.03 g g^{-1}, respectively, outperforming previously reported adsorbents for **BTX** adsorption (Table S4†). In addition to chemical adsorption, **Py-CSSE** displayed fluorescent sensing properties towards dual detection of both Cu (II) and F^- in polar organic solvents, enabling it to function as a hybrid adsorbent and fluorescent sensing material simultaneously.

Experimental

Chemicals

Octavinylsilsesquioxane (**OVS**) was prepared according to the literature report.[43] Commercially available compounds including 1-bromopyrene, triphenylphosphine (PPh_3), triethylamine (NEt_3), tetrabutylammonium salts, all metal perchlorate salts, $Pd(OAc)_2$, EDTA and octamethylcyclotetrasiloxane (**methyl D_4**) were purchased from TCI chemicals and Sigma-Aldrich and used subsequently without further purification. The commercial-grade solvents including DCM, acetone, hexanes, ethyl acetate, and methanol were distilled prior to use. The analytical grade solvents including THF, toluene, isopropanol and DMF were purchased from RCI-Labscan and used without further purification. Deionized (DI) water was obtained from Ultra Clear SIEMENS under ASTM type 1 and 2.

Synthesis

Synthesis of a crosslinked siloxane–silsesquioxane elastomer with pyrene functionalization (Py-CSSE). A mixture of **OVS** (1 g, 1.58 mmol), **Mono-PySQ** (2 mol%, 25 mg, 0.03 mmol) and **methyl D_4** (3 mL, 8.57 mmol) was mixed in DMF (6 mL) in the presence of K_2CO_3 (30 mg, 0.2 mmol). The reaction was stirred at 75 °C until the cloudy solution turned into a clear solution. After 10 minutes, the solution turned into a gel which was subsequently washed sequentially with various solvents (DMF, DI water, CH_2Cl_2, hexane and isopropanol in order) by soaking the product in each solvent for 1 hour. The material surface was modified with 5% of hexamethyldisiloxane (HMDSO) in 50 mL of isopropanol overnight before drying under reduced pressure (Video S1†). The product was obtained in 83%yield.

Study of BTX adsorption. A cubic-shaped sample of **Py-CSSE** ($1 \times 1 \times 1$ cm^3) was exposed to separate vials containing 2 mL of individual organic solvents including hexane, THF, DCM, DMF, EtOH, MeOH, and DI water. The **Py-CSSE** samples were weighed to measure their dry weights (W_d) and the weights of **Py-CSSE** (W_w) after exposure to each organic solvent. The adsorption capacity (q) of **Py-CSSE** for each solvent was deter-

mined by using eqn (1) and reported in terms of g g^{-1} and mol g^{-1}.

$$\text{Adsorption capacity } (q) = (W_w - W_d)/W_d \quad (1)$$

Time-dependent adsorption of **Py-CSSE** was investigated by using *o*-xylene and DI water as representative non-polar and polar solvents, respectively. A cube of **Py-CSSE** was added into a mixture of *o*-xylene (1.0 mL) and DI water (0.5 mL) and the adsorption capacities were calculated at different adsorption times ranging from 15 to 30, 45, 60, and 90 seconds. The maximum adsorption capacity was determined by varying the volume of *o*-xylene (0.25, 0.50, 0.75, 1.0, and 1.25 mL) in 0.5 mL of DI water and the adsorption capacity of each experimental set was calculated at the adsorption time of 90 seconds.

The recyclability of **Py-CSSE** was studied by adding the material into a mixture of *o*-xylene (1.0 mL) and DI water (0.5 mL). The adsorption process was performed for 90 seconds and the adsorption capacity was calculated. In the desorption process, the absorbed liquid was squeezed from the **Py-CSSE** and the **Py-CSSE** was dried at room temperature for 30 minutes before the next cycle.

Fluoride and cyanide adsorption and recyclability of Py-CSSE

Anion adsorption experiments with **Py-CSSE** were carried out using fluoride and cyanide as model anions in this study. In the case of fluoride adsorption, **Py-CSSE** (10 mg) was suspended in THF (2 mL) and a solution of TBAF (0.96 mM) was added subsequently into the suspension. Each solution was collected after adsorption times of 5, 15, 30, 45, and 60 minutes by filtering the **Py-CSSE** residues off from each solution and the remaining solution was collected to determine the amount of fluoride.

In order to determine the concentrations of the remaining fluoride, we used our previously reported hydrazone sensor for the spectrophotometric analysis of fluoride. First of all, a calibration curve was constructed by preparing a series of TBAF solutions in THF with concentrations of 0.2, 0.4, 0.8, 1.2, and 1.6 mM. Each TBAF solution (0.02 mL) was added subsequently into solutions of the sensor (2 mL, 2×10^{-5} M). The signals obtained from each absorption spectrum were plotted as a function of fluoride concentration to create a calibration curve. The sampling solutions collected from all samples were added into a vial containing the solution of the sensor (2 mL, 2×10^{-5} M). The absorption values were collected and the concentrations of fluoride were calculated using a linear equation obtained from the calibration curve. The removal efficiency (% RE) was calculated using the following eqn (2):

$$\%\text{RE} = (C_0 - C_e)/C_0 \times 100 \quad (2)$$

where C_0 and C_e (mg L^{-1}) are the initial and residual concentrations of ions in organic solutions. Cyanide removal capacity was determined through a similar experiment.

Results and discussion

Synthesis and characterization

Py-CSSE was synthesised from **OVS** (1 eq.), **methyl D_4** (6 eq.), and **Mono-PySQ** (2 mol%) *via* anionic ring-opening polymerization in the presence of a base (Scheme 1). The unreacted starting materials were removed by stepwise washing with solvents to afford **Py-CSSE** as the solid product in 83% yield. **Py-CSSE** was insoluble in organic solvents ranging from non-polar to polar solvents, which is in stark contrast to its synthetic precursors, confirming the successful crosslinking polymerization reaction.

The MAS solid-state ^{29}Si-NMR spectrum of **Py-CSSE** revealed a distinct silicon signal at −80 ppm, a characteristic silicon peak of the T_3 species (T_n: $CSi(OSi)_n(OH)_{3-n}$) derived from the silsesquioxane cage. Furthermore, the spectrum also shows a sharp signal around −20 ppm suggesting the presence of the D_2 species (D_n: $(CH_3)_{4-n}Si(O_{1/2})_n$) derived from the polysiloxane chains. The shoulder signal at around −18 ppm potentially could be attributed to a signal of the D structures having different distance distributions to the T structures.[44–49] The MAS solid-state ^{13}C-NMR spectrum of **Py-CSSE** exhibits a signal at 0.9 ppm, corresponding to the sp^3 methyl carbon of siloxane chains. The spectrum also showed broad multiple signals around 132–134 ppm, corresponding to sp^2 carbons derived from the abundant vinyl groups of OVS (Fig. 1b). Importantly, the signals associated with pyrene are absent from the spectrum. This is due to the limited sensitivity of the MAS solid-state ^{13}C-NMR technique, which inhibited the detection of signals resulting from the small amount of **Mono-PySQ** introduced into **Py-CSSE** (Fig. S2†).

The FTIR spectrum of **Py-CSSE** displays the characteristics of a crosslinked siloxane–silsesquioxane elastomer (**CSSE**) and **Mono-PySQ** (Fig. 1c) by showing prominent vibrational peaks at 1072 cm^{-1} and 793 cm^{-1}, which correspond to the stretching and bending frequencies of Si–O–Si, respectively. The results unequivocally verified the existence of Si moieties inside the polymeric network.[50,51] The signal observed at a wavenumber of 968 cm^{-1} is attributed to the bending frequency of the C=C bond in vinyl groups with a pyrene substituent. The absorption signal centred at 3023 cm^{-1} provides evidence for the existence of aromatic pyrenyl groups derived from **Mono-PySQ** and the intensity of the signal strongly correlates with the amount of **Mono-PySQ** additive, and the signal that emerges at 3064 cm^{-1} is attributed to vibrational stretching of C–H vinyl moieties.[52,53] The susceptibility of **POSS** derivatives to bases may lead to a cage structure transformation into a partially-open cage structure.[54–56] This was confirmed by the presence of weak and broad signals of O–H stretching in the range of 3200–3500 cm^{-1} (Fig. 1d and Table S1†).

The crosslinking polymerization significantly changed the crystalline structure of **OVS**, from a well-defined structure to an amorphous solid, as determined by X-ray diffraction analysis.[57] **Py-CSSE** exhibited only two broad signals at 2θ = 11° and 22° (Fig. S4†). According to Bragg's Law, the d_1-spacing for 2θ =

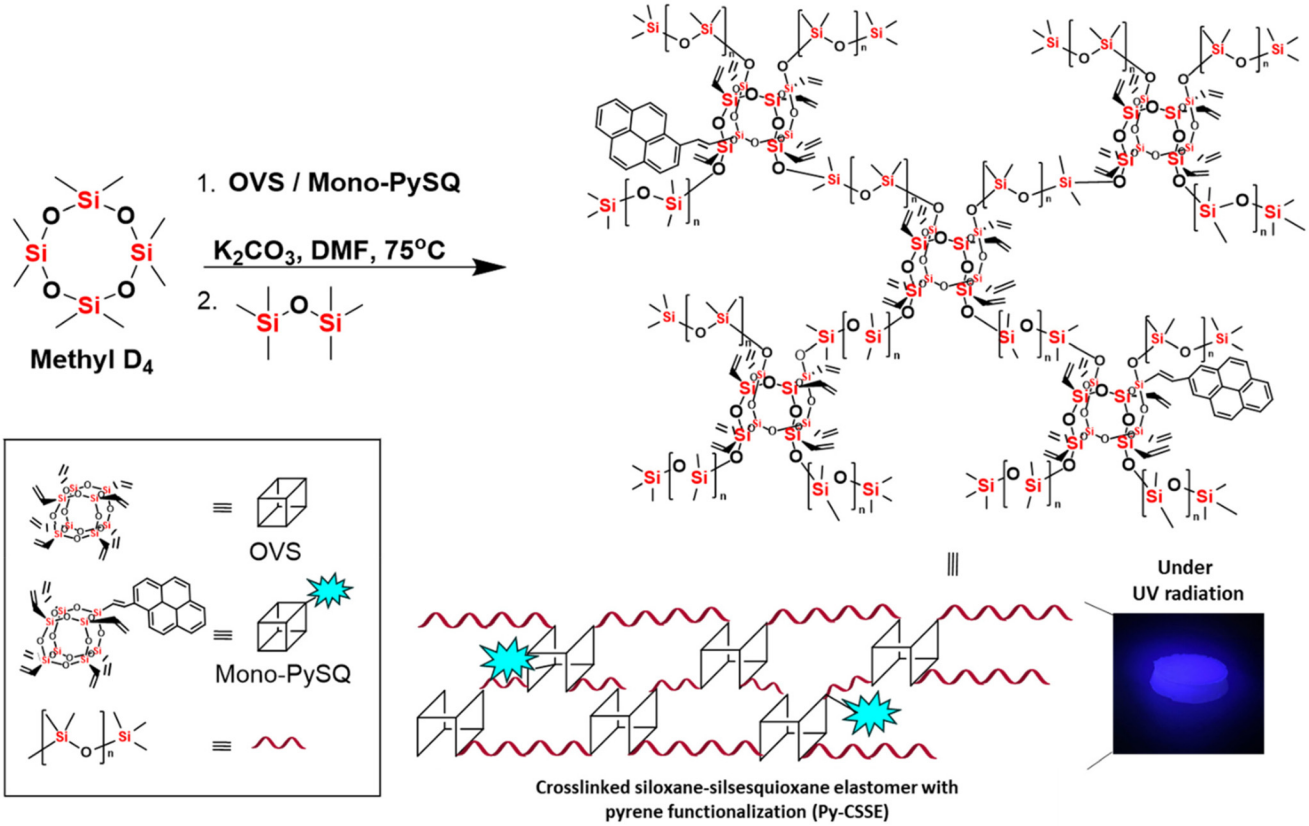

Scheme 1 The synthesis of a crosslinked siloxane–silsesquioxane elastomer with pyrene functionalization (**Py-CSSE**).

11° was approximately 0.81 nm, while the d_2-spacing for 2θ = 22° was 0.41 nm, representing the distance between the Si–O–Si portions of the siloxane chains as amorphous silicone rubber and amorphous cluster, respectively.[23,58] In addition, the d_1-spacing of **Py-CSSE** is slightly shorter than that of **CSSE** (0.98 nm), indicating the strong interactions between each **POSS** layer as a result of stacking of pyrenyl moieties.

Thermogravimetric analysis (TGA) of **Py-CSSE** identified a weight loss occurring in two stages. Under a N_2 atmosphere, an initial weight loss at 300 °C ascribed to the decomposition of organic constituents was observed. The second stage of weight loss took place within the temperature range of 487–531 °C, which can be explained by the decomposition of the Si–O inorganic core structure (Fig. S7†). Importantly, **Py-CSSE** exhibited superior thermal stability in comparison to **OVS**, which decomposed at approximately 274–303 °C (Fig. S5†).[59] Under an O_2 atmosphere, **Py-CSSE** was completely decomposed at 375 °C and gave the resulting ceramic yield of 78%, slightly higher than that of **OVS** itself (70%). This can be explained by the higher Si portions in **Py-CSSE** as a result of the extra siloxane chains from the **methyl D_4** monomer (Fig. S6 and S8†). The DSC analysis of **Py-CSSE** revealed T_g and T_m values at 179 °C and 317 °C, respectively, indicating that **Py-CSSE** changes from an amorphous solid to a rubbery state at 179 °C and is stable up to 300 °C (Fig. S9†).[60]

The morphology of **Py-CSSE** was studied *via* Field Emission Scanning Electron Microscopy (FESEM). The low magnification SEM image revealed the aggregation of microrod structures with a smooth surface. In addition, a uniform coral-like structure was observed in the higher magnification FESEM image (Fig. 2a and S10†). The micro-structures of **Py-CSSE** bear a resemblance to the hairy-structural surface of lotus leaves that contributes to their hydrophobic nature (Fig. 2b). Surprisingly, the contact angle of **Py-CSSE** is 114° (Fig. 2c) while **CSSE**, the previously reported analogous elastomer without the pyrenyl substituents, exhibited a contact angle value of 151°.[61,62] This result is the opposite of our hypothesis that the addition of pyrenyl groups would increase the hydrophobicity of **Py-CSSE**. **Py-CSSE** demonstrates a shorter D_1-spacing than **CSSE** (0.81 nm *vs.* 0.98 nm), indicating that the incorporation of pyrenyl moieties into **Py-CSSE** probably prevents the formation of long siloxane chains between each silsesquioxane unit during polymerization and potentially causes a collapsed structure as a result of the self-assembly disorder, resulting in a lower hydrophobicity.[63] The energy dispersive X-ray (EDX) pattern showed the presence of Si, O, and C atoms which can imply the presence of both the **SQ** cage and pyrene aromatic ring within the polymeric networks (Fig. S11†).

The determination of compressive strength was conducted in order to evaluate the mechanical properties of **Py-CSSE**. The observation that the maximum compressive strength of the

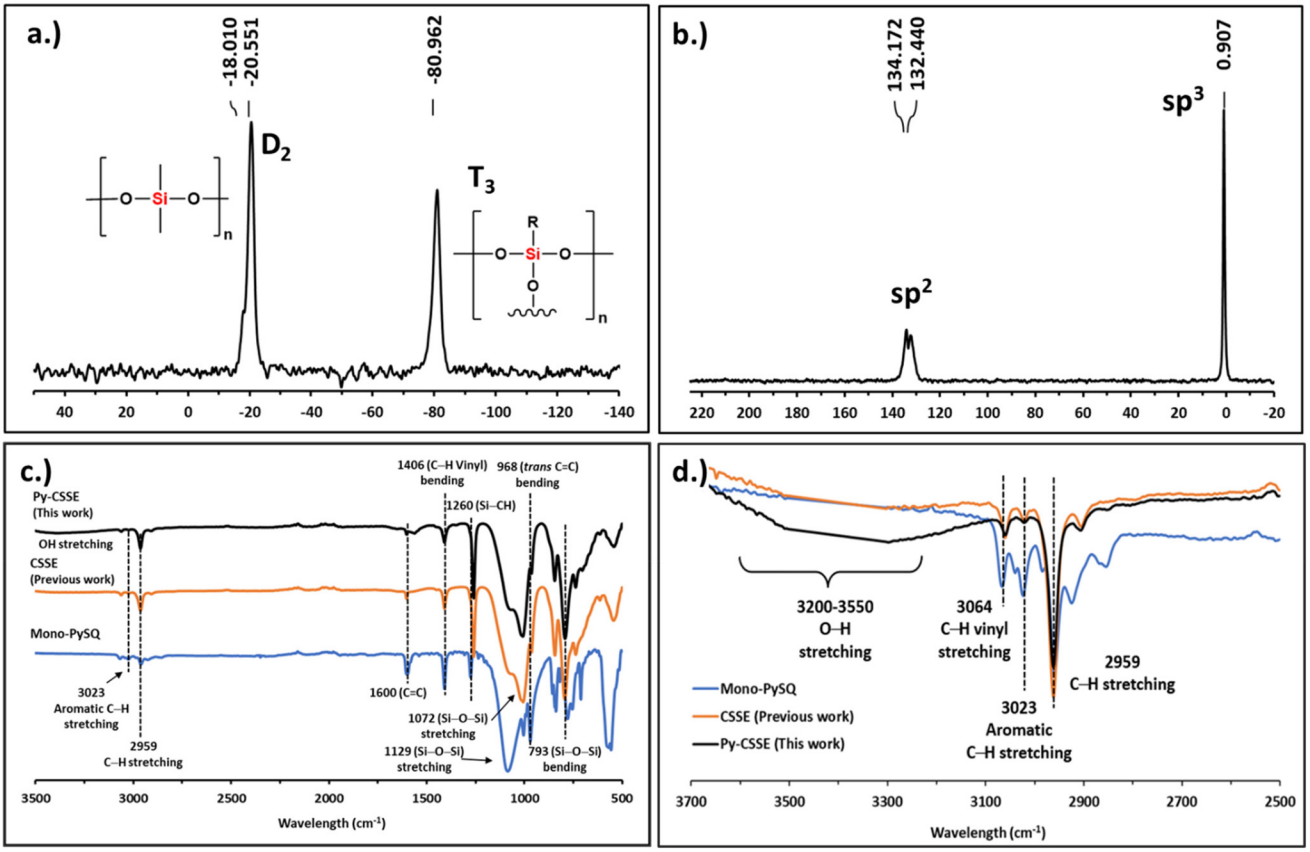

Fig. 1 The MAS solid-state (a) ^{29}Si-NMR spectrum and (b) ^{13}C-NMR spectrum of **Py-CSSE**. (c and d) Comparative FTIR spectra of **Mono-PySQ** (blue), **CSSE** (orange) and **Py-CSSE** (black) samples.

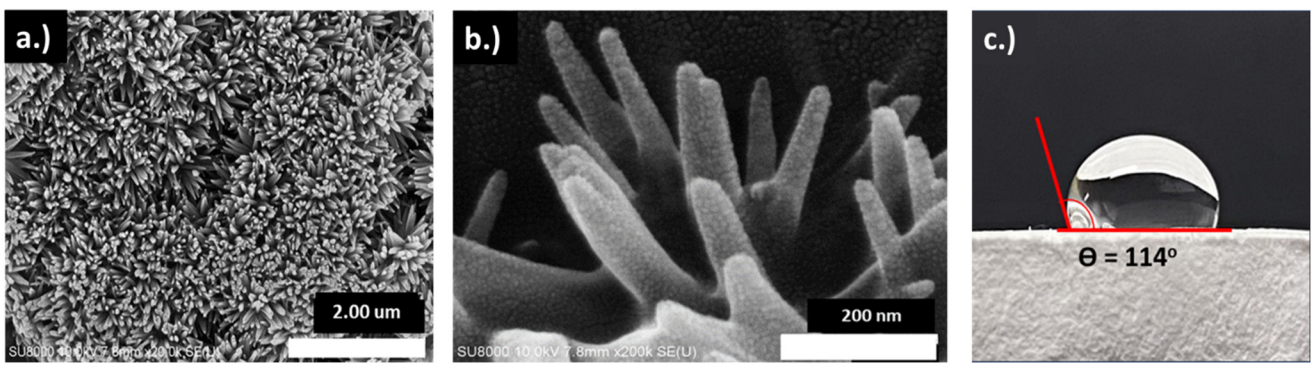

Fig. 2 (a and b) FESEM images of a dried **Py-CSSE**. (c) The contact angle and wettability measurement of **Py-CSSE**.

sample increased up to 60% strain indicates that **Py-CSSE** is quite flexible presumably influenced by the presence of siloxane chains (Fig. S12b†).[64,65] Furthermore, it exhibited notable flexibility without experiencing any cracking during three compressive tests conducted under an applied stress of 40% strain (Fig. S12c†).[66,67]

Photophysical properties of Py-CSSE

The solid-state fluorescence emission properties of **Py-CSSE** were preliminarily inspected under UV-light. Only **Py-CSSE** and **Mono-PySQ** exhibited fluorescence emission while **OVS** and **CSSE** did not show such a response. Subsequently, **Py-CSSE** was suspended in polar organic solvents including THF, DMF and DMSO and excited at wavelengths of 355, 360, and 370 nm, respectively (Fig. 3b). **Py-CSSE** showed a similar pattern of emission spectra which have emission signals of the monomeric pyrene centered at the wavelength around 397 nm and those of the excimeric pyrene centered at the wavelengths around 419 and 443 nm.[68,69] Notably, it is obviously observed

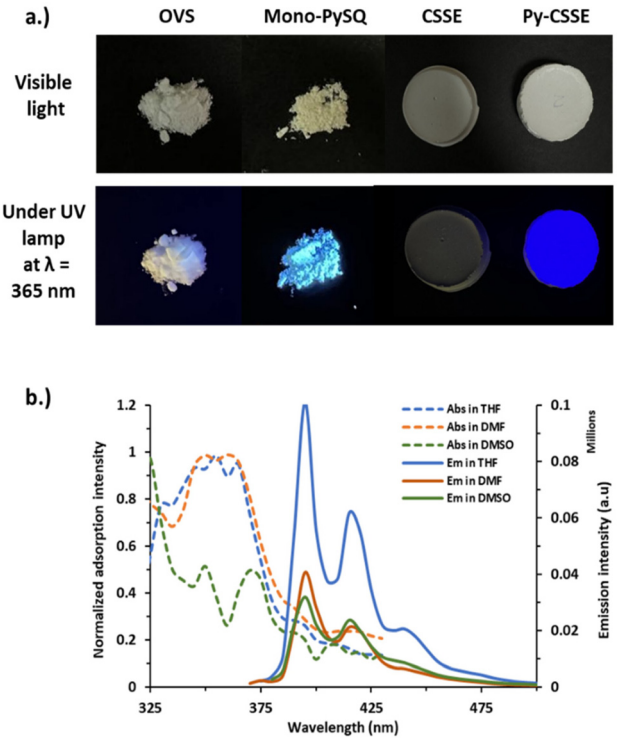

Fig. 3 (a) Solid-state fluorescent emission of **OVS**, **Mono-PySQ**, **CSSE**, and **Py-CSSE** under visible light and UV light at λ_{ex} = 365 nm. (b) Absorption and emission spectra of **Py-CSSE** (1 mg mL^{-1}) in THF, DMF, and DMSO.

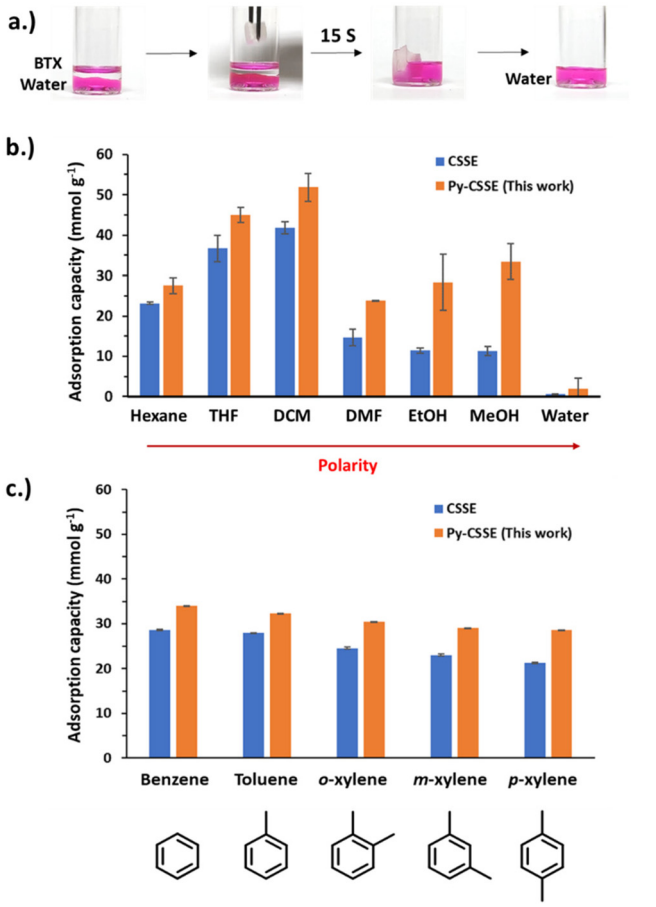

Fig. 4 (a) A diagram showing **BTX** adsorption on water containing a rhodamine B dye by **Py-CSSE**. Adsorption capacities of **Py-CSSE** and **CSSE** towards (b) various solvents reported in mmol g^{-1} and (c) **BTX** reported in mmol g^{-1}.

that the ratio of the emission intensity between the pyrene excimer and monomer (I_{ex}/I_{mo}) increased when the concentration of **Py-CSSE** increased. This observation suggests that the excimer formation of pyrene becomes more prevalent at high concentration due to the closer proximity of molecules (Fig. S13 and Table S2†).[70] In addition, pyrene is non-polar and likely to aggregate in high polarity solvents.[36]

Adsorption efficiency of Py-CSSE

BTX adsorption efficiency of Py-CSSE. **Py-CSSE** can potentially be used as an adsorbent for oil and non-polar solvents as a result of its hydrophobicity. The solvent adsorption experiments were conducted in water, oil, and organic solvents including hexane, THF, DCM, DMF, ethanol, and methanol to evaluate its adsorption efficiency. The results suggest that **Py-CSSE** exhibited adsorption capacities spanning from 2–52 mmol g^{-1}, depending on solvent polarity (Fig. 4b). Notably, in DCM, **Py-CSSE** demonstrated the highest adsorption capacity recorded at 52 mmol g^{-1}. However, **Py-CSSE**'s adsorption efficiency in high polarity solvents such as DMF, EtOH, MeOH, and especially DI water is limited due to its hydrophobic nature. Importantly, **Py-CSSE** showed superior adsorption for all organic solvents to **CSSE**, the pyrene-free analogue, under the same conditions (Table S3†).

Due to the remarkable hydrophobic properties of **Py-CSSE**, we proceeded to conduct more challenging studies on the adsorption of benzene, toluene, and xylenes (**BTX**). First of all, a cube-shaped piece of **Py-CSSE** (1 × 1 × 1 cm^3) was immersed in an aqueous solution of rhodamine B dye that was layered with the organic solvent of interest (Fig. 4a). **Py-CSSE** demonstrated a maximum adsorption capacity of 34.02, 32.34, 30.46, 28.98, and 28.56 mmol g^{-1} for benzene, toluene, *o*-xylene, *m*-xylene, and *p*-xylene, respectively (Fig. 4c). Interestingly, despite showing less hydrophobicity than **CSSE**, **Py-CSSE** showed higher solvent and **BTX** adsorption capacities, highlighting the benefit of having the pyrenyl moieties within the material matrix.

Furthermore, the kinetics of *o*-xylene adsorption in the presence of DI water were also studied. **Py-CSSE** was exposed to a mixture of *o*-xylene and DI water, and the percentage of swelling was measured at several intervals in the adsorption experiments, specifically 15, 30, 45, 60, and 90 seconds. The results indicate that only *o*-xylene was absorbed, and the adsorption nearly reached saturation during the initial 30 seconds and almost complete (~100%) removal of **BTX** within

a timeframe of 90 seconds (Fig. 4a and S15†). **Py-CSSE** demonstrated a maximum adsorption capacity for *o*-xylene of 3.23 g g^{-1} or 30.46 mmol g^{-1}. Additionally, it displayed a swelling percentage of 315% after attaining adsorption saturation (Fig. 5a). These results demonstrate that **Py-CSSE** had exceptional performance in **BTX** adsorption compared to other inorganic adsorbents and porous materials (*i.e.* SBA-15) previously documented (Table S4†). In order to be suitable for practical industrial use, it is necessary for the adsorbent to be capable of being recycled. We conducted multiple dynamic breakthrough experiments using the **Py-CSSE** material to study the adsorption of the mixture of *o*-xylene and DI water. The adsorption process lasted for 90 seconds, after which the sample was dried at room temperature for approximately 30 minutes. The recycling studies demonstrated consistent levels of both adsorption efficiency and quantity over five adsorption–desorption cycles (Fig. 5b).

Py-CSSE as an anion and cation sensor. Our group has previously reported the use of silsesquioxane-based materials in anion sensing applications.[35,36] In this work, the investigation of the fluorescent anion sensing properties of **Py-CSSE** was initially carried out by adding individual anions including F^-, Cl^-, Br^-, I^-, NO_3^-, CN^-, SCN^-, HSO_4^-, and ClO_4^- as their tetrabutylammonium (TBA) salts into the suspension of **Py-CSSE** in THF. The naked-eye observations and images taken from the epifluorescent microscopy suggested that only F^- and CN^- exhibited dramatic quenching of the **Py-CSSE** fluorescence signals, while other anions failed to give similar changes (Fig. 6a and c). Our previous studies revealed that both F^- and CN^- exhibited the quenching of emission signals derived from **Mono-PySQ**. It is likely that F^- and CN^- interact with the electropositive vinylene-silicon centers of the silsesquioxane cage. This process results in the formation of intramolecular charge-transfer (ICT) complexes which caused the quenching of the fluorescence emission signals.[42,71–73] Fluorescent anion titration experiments determined the detection limits for F^- and CN^- sensing to be on the nanomolar scale (Fig. 6e and f, Table S5†). In addition, the pseudo-first order kinetic rate constants for the two ions were calculated to be 2.1×10^{-3} and 8.8×10^{-3} s^{-1}, respectively (Fig. 6e and f insets, S20 and Table S6†).

In addition to anion sensing, the fluorescent cation sensing properties of **Py-CSSE** were explored in relation to specific transition metals, namely Cr^{2+}, Mn^{2+}, Fe^{2+}, Co^{2+}, Cu^{2+}, Zn^{2+}, and Cd^{2+} in the form of their perchlorate salts in THF. The presence of Cu^{2+} caused a substantial suppression of the fluorescence signal of **Py-CSSE**, as confirmed by both naked-eye observation and epifluorescent microscope images (Fig. 6b, d and S28†). According to previous reports on fluorescence sensors based on the pyrene fluorophore, fluorescence quenching is caused by the paramagnetic nature of Cu^{2+} and ligand-to-metal charge transfer (LMCT) processes that are highly selective and sensitive to Cu^{2+}, particularly with ligands containing nitrogen and oxygen donor atoms.[74] Furthermore, Cu^{2+} sensing yielded LOD and LOQ values of 2.72 and 8.23 nM, respectively (Table S5†). In order to examine the kinetics of Cu^{2+} adsorption, variations in fluorescence intensity in THF were monitored. The signals of fluorescence remained relatively constant after 15 minutes. Furthermore, the pseudo-first order kinetic rate constant was determined to be 5.1×10^{-3} s^{-1} (Fig. 6g inset and Table S6†).

Fluoride and cyanide adsorption. **Py-CSSE** has emerged as a highly promising candidate for the removal of toxic F^- and CN^- ions in environmental remediation applications as a result of strong and complementary interactions between these highly basic anions with the Si center in **POSS** motifs (Fig. 7).[34,56] **Py-CSSE** was found to adsorb approximately 80% of the fluoride and cyanide ions from each anion solution within a duration of 5 minutes (Fig. S24a†). The recyclability of the **Py-CSSE** adsorbent was assessed by subjecting it to F^- adsorption in accordance with the experimental protocol described above. The fluoride removal capacities of **Py-CSSE** were approximately 60–70% during the first and subsequent cycles. However, following the third cycle, the capacity decreased to 40% (Fig. S24b†). The results subtly indicated that F^- ions were irreversibly and strongly bound to the silsesquioxane cage.[75,76]

Copper(II) adsorption. The adsorption efficiency of Cu^{2+} on **Py-CSSE** was only 35% potentially due to the presence of weak electrostatic interactions between Cu^{2+} and partial cleavage of the cage in **Py-CSSE** (Fig. 7). The FTIR spectrum of **Py-CSSE** + **Cu^{2+}** showed the absence of the O–H stretching signal in the range 3100–3600 cm^{-1} (Fig. S21†). Presumably, the Cu^{2+} ions were bound to the **Py-CSSE** frameworks by coordinating with

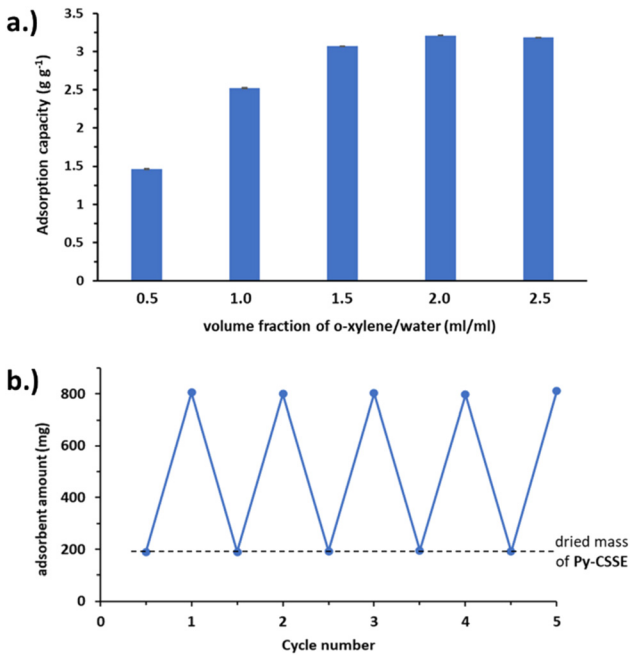

Fig. 5 (a) Adsorption capacity of **Py-CSSE** at different amounts of *o*-xylene. (b) The recyclability of **Py-CSSE** for the adsorption of *o*-xylene.

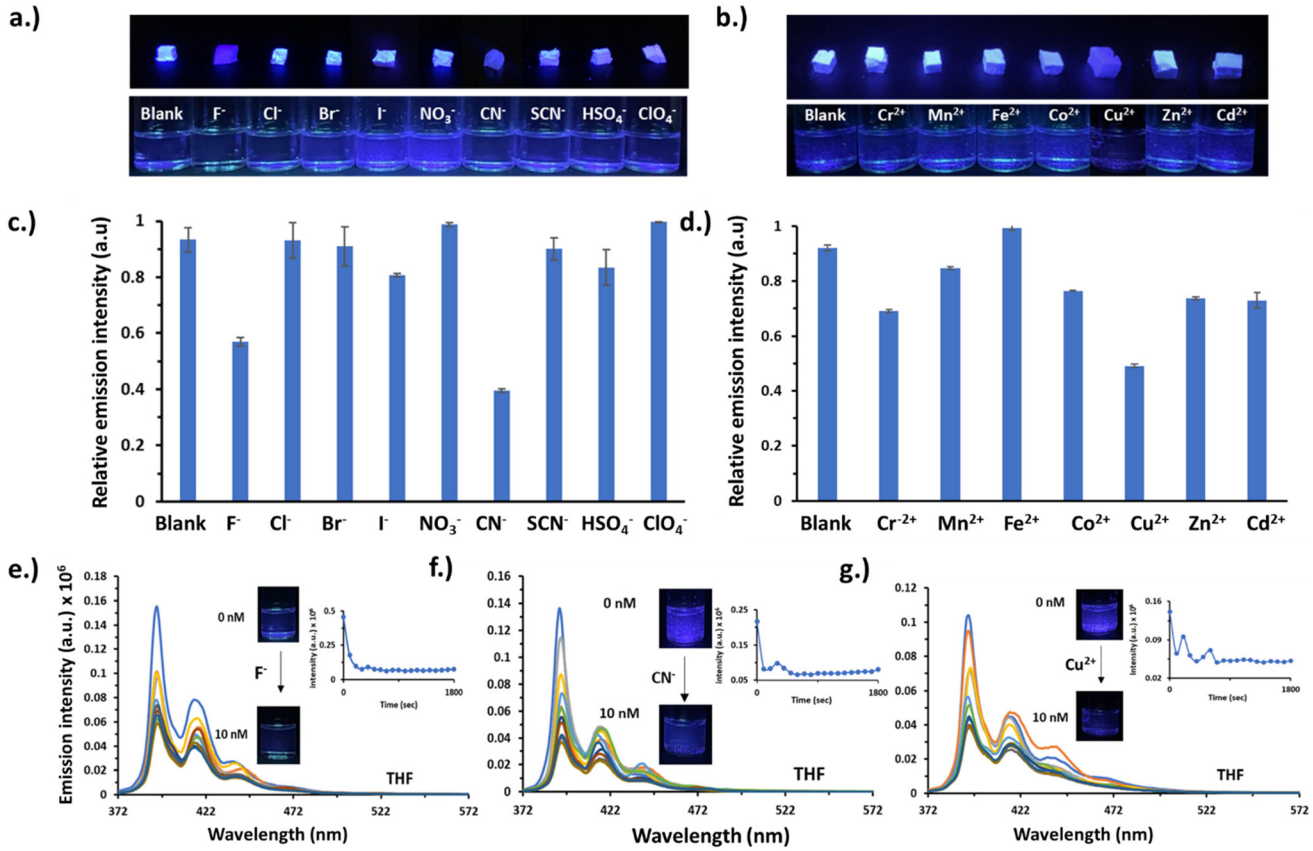

Fig. 6 (a) Photograph of **Py-CSSE** in both solid state and suspension in THF before and after adding anions as their TBA^+ salts and (b) cations as their ClO_4^- salts. Bar graphs representing the relative emission intensity of the **Py-CSSE** suspension in THF in the presence of (c) anions and (d) cations. Fluorescence emission spectra of **Py-CSSE** upon titrations with (e) TBAF, (f) TBACN, and (g) $Cu(ClO_4)_2$ in THF (inset: kinetic plots of fluorescence quenching of **Py-CSSE** upon addition of an excess of TBAF, TBACN, and $Cu(ClO_4)_2$).

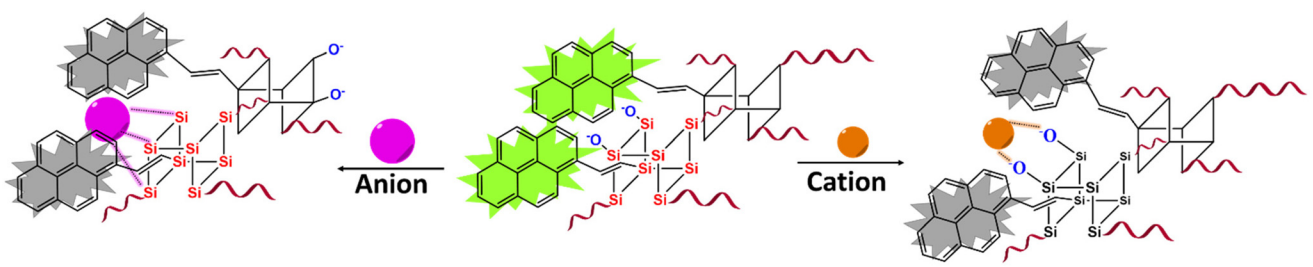

Fig. 7 Schematic illustration of the sensing mechanism for anions and cations.

the electronegative oxygen atoms of silanol groups. **Py-CSSE** underwent a transformation from a spiky to a rounder surface after being subjected to the adsorption of Cu^{2+}. Furthermore, the size of **Py-CSSE** changed from 50 nm to 500 nm after Cu^{2+} adsorption (Fig. S25a and S25b†).[77,78] SEM-EDX analysis revealed that only 4% Cu was found on the surface of **Py-CSSE** (Fig. S26 and S27†). In addition, upon adsorption of Cu^{2+} on the **Py-CSSE** polymer, a noticeable transition from emissive to non-emissive behaviors was seen at 350 nm using epifluorescence microscopy (Fig. S28†).

Conclusions

A crosslinked siloxane/silsesquioxane elastomer with pyrene functionalization (**Py-CSSE**), a novel fluorescent elastomer, was effectively synthesised through the base catalysed one-pot anionic ring-opening polymerization affording the target elastomeric product in a high yield within 10 minutes. **Py-CSSE** displayed chemical characteristics similar to those of **CSSE** and **Mono-PySQ** confirmed by a suite spectroscopic techniques such as FTIR and MAS-NMR. In addition, **Py-CSSE** demon-

strated significant elasticity and can quickly return to its initial shape without any cracking, even when subjected to a pressure range of up to 40% strain for 3 cycles. The solid state and suspension in organic solvent of **Py-CSSE** displayed intense fluorescence emissions, which can be attributed to the pre-functionalization of pyrene molecules as the fluorophore in this crosslinking elastomer. The simultaneous presence of silsesquioxane cages, siloxanes, and pyrene moieties in **Py-CSSE** permitted its use as a dual sensor for anions (F^- and CN^-) and cations (Cu^{2+}) in polar organic media. Furthermore, **Py-CSSE** could also display a capability for cation and anion adsorption. Importantly, it is noteworthy that **Py-CSSE** exhibited a notable adsorption efficiency towards benzene, toluene, and xylenes (**BTX**) and can function as an adsorbent for solvent separation more than five times. Its distinctive structural attributes render it highly suitable for tackling obstacles encountered in the petrochemical sector, environmental remediation, and other analogous implementations.

Author contributions

The manuscript was written through contributions of all authors. All authors have given approval to the final version of the manuscript.

Data availability

Data for this article, including NMR, IR, SEM, XPS, compression testing, XRD, and adsorption data, are available at Open Science Framework at **https://doi.org/10.17605/OSF.IO/RKB7N**.

Conflicts of interest

There are no conflicts to declare.

Acknowledgements

This project was funded by the National Research Council of Thailand (NRCT) and Mahidol University (Basic Research Fund: fiscal year 2023). T. B. and V. E. thank the Center of Excellence for Innovation in Chemistry (PERCH-CIC), Ministry of Higher Education, Science, Research and Innovation and the Office of the Permanent Secretary, Ministry of Higher Education, Science, Research and Innovation (Grant No. RGNS 65-150) for financial support. M. S. is thankful for funding from the National Research Council of Thailand (NRCT, N42A661000).

References

1 M. K. S. Nascimento, S. Loureiro, M. R. d. R. Souza, M. d. R. Alexandre and J. Nilin, *Mar. Pollut. Bull.*, 2020, **156**, 111272.
2 A. Mirzaei, J.-H. Kim, H. W. Kim and S. S. Kim, *J. Mater. Chem. C*, 2018, **6**, 4342–4370.
3 J. C.-S. Wu, Z.-A. Lin, F.-M. Tsai and J.-W. Pan, *Catal. Today*, 2000, **63**, 419–426.
4 E. R. L. Tiburtius, P. Peralta-Zamora and A. Emmel, *J. Hazard. Mater.*, 2005, **126**, 86–90.
5 A. Torabian, H. Kazemian, L. Seifi, G. N. Bidhendi, A. A. Azimi and S. K. Ghadiri, *Clean: Soil, Air, Water*, 2010, **38**, 77–83.
6 S. Štandeker, Z. Novak and Ž. Knez, *J. Hazard. Mater.*, 2009, **165**, 1114–1118.
7 A. Aleghafouri, N. Hasanzadeh, M. Mahdyarfar, A. SeifKordi, S. M. Mahdavi and A. T. Zoghi, *J. Nat. Gas Sci. Eng.*, 2015, **22**, 618–624.
8 G. Hayase, K. Kanamori, M. Fukuchi, H. Kaji and K. Nakanishi, *Angew. Chem., Int. Ed.*, 2013, **52**, 1986–1989.
9 B. Buszewski, R. M. Gadzała-Kopciuch, M. Markuszewski and R. Kaliszan, *Anal. Chem.*, 1997, **69**, 3277–3284.
10 H. Qiu, X. Liang, M. Sun and S. Jiang, *Anal. Bioanal. Chem.*, 2011, **399**, 3307–3322.
11 V. Lenher and H. B. Merrill, *J. Am. Chem. Soc.*, 1917, **39**, 2630–2638.
12 L. Spitzmüller, F. Nitschke, B. Rudolph, J. Berson, T. Schimmel and T. Kohl, *J. Nanopart. Res.*, 2023, **25**, 40.
13 J. R. Jagannathan, K. Targos and A. K. Franz, *Angew. Chem.*, 2022, **134**, e202110417.
14 T. Jaroentomeechai, P.-k. Yingsukkamol, C. Phurat, E. Somsook, T. Osotchan and V. Ervithayasuporn, *Inorg. Chem.*, 2012, **51**, 12266–12272.
15 J. Kaźmierczak, D. Lewandowski and G. Hreczycho, *Inorg. Chem.*, 2020, **59**, 9206–9214.
16 M. G. Mohamed and S.-W. Kuo, *Soft Matter*, 2022, **18**, 5535–5561.
17 T. Hamada, S. Takase, A. Tanaka, K. Okada, S. Mineoi, A. Uedono and J. Ohshita, *ACS Appl. Polym. Mater.*, 2022, **5**, 743–750.
18 T. Hamada, Y. Nakanishi, K. Okada, S. Tsukada, A. Uedono and J. Ohshita, *ACS Appl. Polym. Mater.*, 2021, **3**, 3383–3391.
19 X. Chen, L. Li, T. Wei, D. C. Venerus and J. M. Torkelson, *ACS Appl. Mater. Interfaces*, 2018, **11**, 2398–2407.
20 S. Bourbigot, T. Turf, S. Bellayer and S. Duquesne, *Polym. Degrad. Stab.*, 2009, **94**, 1230–1237.
21 W. Zhang, G. Camino and R. Yang, *Prog. Polym. Sci.*, 2017, **67**, 77–125.
22 H. Chen, S. Wei, R. Wang and M. Zhu, *ACS Biomater. Sci. Eng.*, 2021, **7**, 1428–1437.
23 S. O. Hwang, J. Y. Lee and J.-H. Lee, *Prog. Org. Coat.*, 2019, **137**, 105316.
24 M. Ejaz, M. M. Samy, Y. Ye, S.-W. Kuo and M. G. Mohamed, *Int. J. Mol. Sci.*, 2023, **24**, 2501.

25 T. K. L. Nguyen, T. N. Phan, F. Cousin, D. Devaux, S. Mehan, F. Ziarelli, S. Viel, D. Gigmes, P. Soudant and R. Bouchet, *Chem. Mater.*, 2022, **34**, 6944–6957.
26 R. Yanagisawa, H. Endo, M. Unno, H. Morimoto and S.-i. Tobishima, *J. Power Sources*, 2014, **266**, 232–240.
27 H. Zhang, S. Kulkarni and S. L. Wunder, *J. Phys. Chem. B*, 2007, **111**, 3583–3590.
28 P. K. Behera, P. Mondal and N. K. Singha, *Macromolecules*, 2018, **51**, 4770–4781.
29 Z. Zhao, Y. Ma, P. Ju, Y. Wu, L. Chen, H. Zhou and J. Chen, *ACS Appl. Mater. Interfaces*, 2022, **14**, 36105–36115.
30 R. Y. Kannan, H. J. Salacinski, P. E. Butler and A. M. Seifalian, *Acc. Chem. Res.*, 2005, **38**, 879–884.
31 A. Birault, E. Molina, G. Toquer, P. Lacroix-Desmazes, N. Marcotte, C. Carcel, M. Katouli, J. R. Bartlett, C. Gerardin and M. W. C. Man, *ACS Appl. Bio Mater.*, 2018, **1**, 1787–1792.
32 T. Shimizu, K. Kanamori and K. Nakanishi, *Chem. – Eur. J.*, 2017, **23**, 5176–5187.
33 C. Wannasiri, S. Chanmungkalakul, T. Bureerug, M. Sukwattanasinitt and V. Ervithayasuporn, *Chem. Commun.*, 2023, **59**, 5471–5474.
34 C. Wannasiri, S. Chanmungkalakul, T. Bunchuay, L. Chuenchom, K. Uraisin, V. Ervithayasuporn and S. Kiatkamjornwong, *ACS Appl. Polym. Mater.*, 2020, **2**, 1244–1255.
35 S. Chanmungkalakul, V. Ervithayasuporn, P. Boonkitti, A. Phuekphong, N. Prigyai, S. Kladsomboon and S. Kiatkamjornwong, *Chem. Sci.*, 2018, **9**, 7753–7765.
36 S. Chanmungkalakul, V. Ervithayasuporn, S. Hanprasit, M. Masik, N. Prigyai and S. Kiatkamjornwong, *Chem. Commun.*, 2017, **53**, 12108–12111.
37 Z. Gou, X. Zhang, Y. Zuo, M. Tian, B. Dong, Y. Tang and W. Lin, *Sens. Actuators, B*, 2021, **338**, 129837.
38 P. Beyazkilic, A. Yildirim and M. Bayindir, *ACS Appl. Mater. Interfaces*, 2014, **6**, 4997–5004.
39 Q. Wang, M. Unno and H. Liu, *J. Mater. Chem. A*, 2024, **12**, 5679–5691.
40 Y. Lin, T. B. Kouznetsova and S. L. Craig, *J. Am. Chem. Soc.*, 2019, **142**, 99–103.
41 A. S. Fawcett, T. C. Hughes, L. Zepeda-Velazquez and M. A. Brook, *Macromolecules*, 2015, **48**, 6499–6507.
42 P. Siripanich, T. Bureerug, S. Chanmungkalakul, M. Sukwattanasinitt and V. Ervithayasuporn, *Organometallics*, 2022, **41**, 201–210.
43 L. Sun, Z. Liang and J. Yu, *Polym. Chem.*, 2015, **6**, 917–924.
44 I. S. Protsak, Y. M. Morozov, W. Dong, Z. Le, D. Zhang and I. M. Henderson, *Nanoscale Res. Lett.*, 2019, **14**, 1–15.
45 S. Roualdes, R. Berjoan and J. Durand, *Sep. Purif. Technol.*, 2001, **25**, 391–397.
46 Y. Liu, N. Takeda, A. Ouali and M. Unno, *Inorg. Chem.*, 2019, **58**, 4093–4098.
47 Y. Liu, M. Kigure, K. Koizumi, N. Takeda, M. Unno and A. Ouali, *Inorg. Chem.*, 2020, **59**, 15478–15486.
48 J. Kaźmierczak, K. Kuciński and G. Hreczycho, *Inorg. Chem.*, 2017, **56**, 9337–9342.
49 V. M. Litvinov, H. Barthel and J. Weis, *Macromolecules*, 2002, **35**, 4356–4364.
50 T. Tokunaga, S. Koge, T. Mizumo, J. Ohshita and Y. Kaneko, *Polym. Chem.*, 2015, **6**, 3039–3045.
51 D.-S. Ruan, Y.-L. Li, L. Wang, D. Su and F. Hou, *J. Sol-Gel Sci. Technol.*, 2010, **56**, 184–190.
52 M. Xue, X. Zhang, Z. f. Wu, H. Wang, X. Ding and X. y. Tian, *Chin. J. Chem. Phys.*, 2013, **26**, 445–450.
53 D. Chen, W. Sun, C. Qian, L. M. Reyes, A. P. Y. Wong, Y. Dong, J. Jia, K. K. Chen and G. A. Ozin, *Adv. Funct. Mater.*, 2016, **26**, 5102–5110.
54 S. Hanprasit, N. Tungkijanansin, A. Prompawilai, S. Eangpayung and V. Ervithayasuporn, *Dalton Trans.*, 2016, **45**, 16117–16120.
55 F. Olivero, F. Renò, F. Carniato, M. Rizzi, M. Cannas and L. Marchese, *Dalton Trans.*, 2012, **41**, 7467–7473.
56 M. Laird, P. Gaveau, P. Trens, C. Carcel, M. Unno, J. R. Bartlett and M. W. C. Man, *New J. Chem.*, 2021, **45**, 4227–4235.
57 H. Liu and H. Liu, *J. Mater. Chem. A*, 2017, **5**, 9156–9162.
58 J. T. Leem, W. C. Seok, J. B. Yoo, S. Lee and H. J. Song, *Polymers*, 2021, **13**, 1564.
59 H. Vakili, M. Mohseni and E. Mohajerani, *J. Optoelectron. Adv. Mater.*, 2014, **16**, 1031–1038.
60 N. Prigyai, S. Chanmungkalakul, M. Sukwattanasinitt and V. Ervithayasuporn, *New J. Chem.*, 2021, **45**, 14141–14148.
61 N. C. Escudé and E. Y.-X. Chen, *Chem. Mater.*, 2009, **21**, 5743–5753.
62 W.-B. Zhang, Y. Li, X. Li, X. Dong, X. Yu, C.-L. Wang, C. Wesdemiotis, R. P. Quirk and S. Z. Cheng, *Macromolecules*, 2011, **44**, 2589–2596.
63 A. A. Widati, M. Z. Fahmi, S. C. W. Sakti, T. A. Budiastanti and T. E. Purbaningtias, *J. Manuf. Mater.*, 2022, **6**, 110.
64 G. Hayase, K. Kanamori, G. Hasegawa, A. Maeno, H. Kaji and K. Nakanishi, *Angew. Chem., Int. Ed.*, 2013, **52**, 10788–10791.
65 G. Hayase, K. Kanamori and K. Nakanishi, *J. Mater. Chem.*, 2011, **21**, 17077–17079.
66 P. Wojciechowska, R. Cierpiszewski and H. Maciejewski, *Appl. Sci.*, 2022, **12**, 1258.
67 L. Wang, R. Guo, J. Ren, G. Song, G. Chen, Z. Zhou and Q. Li, *Ceram. Int.*, 2020, **46**, 10362–10369.
68 S. Pirouz and J. Duhamel, *J. Polym. Sci., Part B: Polym. Phys.*, 2017, **55**, 7–18.
69 S. Karuppannan and J. C. Chambron, *Chem. – Asian J.*, 2011, **6**, 964–984.
70 Z. Kowser, U. Rayhan, T. Akther, C. Redshaw and T. Yamato, *Mater. Chem. Front.*, 2021, **5**, 2173–2200.
71 D. C. Santra, M. K. Bera, P. K. Sukul and S. Malik, *Chem. – Eur. J.*, 2016, **22**, 2012–2019.
72 G. G. Aloisi, F. Masetti and U. Mazzucato, *Chem. Phys. Lett.*, 1974, **29**, 502–505.
73 W. Thongyod, C. Buranachai, T. Pengpan and C. Punwong, *Phys. Chem. Chem. Phys.*, 2019, **21**, 16258–16269.
74 Z. Kowser, U. Rayhan, T. Akther, C. Redshaw and T. Yamato, *Mater. Chem. Front.*, 2021, **5**, 2173–2200.

75 M. Ronchi, S. Sulaiman, N. Boston and R. M. Laine, *Appl. Organomet. Chem.*, 2010, **24**, 551–557.
76 H. Oda, M. Sato, Y. Morizawa, K. Oshima and H. Nozaki, *Tetrahedron*, 1985, **41**, 3257–3268.
77 Q. Shu, W. Qiu, M. Luo and L. Xiao, *Mater. Today Sustainability*, 2022, **17**, 100094.
78 A. Deptula, J. Rangel-Galera and R. M. Espinosa-Marzal, *Adv. Funct. Mater.*, 2023, **33**, 2300896.